ELSEVIER

Biophysical Chemistry 91 (2001) 281–304

Biophysical Chemistry

www.elsevier.com/locate/bpc

Duplication and extension of the Thorneley and Lowe kinetic model for *Klebsiella pneumoniae* nitrogenase catalysis using a MATHEMATICA software platform

P.E. Wilson, A.C. Nyborg, G.D. Watt*

Department of Chemistry and Biochemistry, Brigham Young University, Provo, UT 84604, USA

Received 24 January 2001; received in revised form 21 May 2001; accepted 31 May 2001

Abstract

The Thorneley and Lowe kinetic model for nitrogenase catalysis was developed in the early to mid 1980s, and has been of value in accounting for many aspects of nitrogenase catalysis. It has also been of value by providing a model for predicting new catalytic behavior. Since its original publication, new results have been obtained and have been successfully incorporated into the model. However, the computer program used for nitrogenase simulations has not been generally available. Using kinetic schemes and assumptions previously outlined by Thorneley and Lowe, we report attempts to duplicate the original T&L kinetic simulation for *Klebsiella pneumoniae* nitrogenase catalysis using an updated simulation based on the MATHEMATICA programming format, which makes it more user-friendly and more readily available. Comparisons of our simulations with the original T&L simulations are generally in agreement, but in some cases serious discrepancy is observed. Possible reasons for the differences are discussed. In addition to duplicating the original T&L model, we report effects of updating it by including information that has come to light subsequent to its original publication. © 2001 Elsevier Science B.V. All rights reserved.

Keywords: Computer simulation; Nitrogenase kinetics; Product distribution; Catalytic efficiency

* Corresponding author. Tel.: +1-801-378-4561; fax: +1-801-378-5474.
E-mail address: gdwatt@chemdept.byu.edu (G.D. Watt).

0301-4622/01/$ - see front matter © 2001 Elsevier Science B.V. All rights reserved.
PII: S0301-4622(01)00182-X

1. Introduction

Biological nitrogen fixation is the conversion of atmospheric nitrogen into ammonia ($N_2 + 6H^+ + 6e^- = 2NH_3$) and is catalyzed by nitrogenase, consisting of the MoFe and Fe proteins [1–4]. In vitro nitrogenase activity is similar in all organisms [5,6] and requires the interaction of the two protein components, a low-potential source of electrons, MgATP and a substrate. The Fe protein binds two MgATPs and, with dithionite as reductant, functions using the $[Fe_4S_4]^{2+}/[Fe_4S_4]^{1+}$ redox couple [5,7] to transfer a single electron to the MoFe protein, with concomitant hydrolysis of two MgATPs. The MoFe protein contains the reductase site [8,9] where electrons accumulate for substrate reduction.

Several kinetic models [8,10,11] have been reported that successfully describe specific but limited aspects of nitrogenase activity, such as activity as a function of component protein concentration and ratio over wide ranges. The most comprehensive kinetic model currently used to describe nitrogenase catalysis is the Thorneley and Lowe (T&L) model, the bulk of which was published in 1985 [5]. However, this source is not a complete reference. Rather, key assumptions and modifications to the original T&L model have appeared in various manuscripts, published prior to and subsequent to this 1985 source [12–19]. Therefore, there is not a single location containing all of the assumptions necessary to duplicate and apply the T&L model. It is of value to have an updated version of the model in a convenient programming format to expand its applicability to new experimental results and the reanalysis of previously reported results.

The differential equations describing the T&L model do not have an analytical solution, so they must be solved numerically. This has been carried out previously using a program written in FORTRAN, which has been available almost exclusively to its authors, due to the fact that code itself is not written in a user-friendly format. These inconveniences provided the impetus for duplicating the T&L model in a modern, user-friendly format (in the MATHEMATICA programming language).

A valuable side-effect of attempting to duplicate the T&L model has been the enumeration of all of its assumptions, both explicit and implied. This is especially important considering that some assumptions and modifications have been added subsequent to the original development of the model [17,19]. These have not been previously tested nor fully justified in terms of their effect on the original kinetic simulations, but we are now able to do so.

2. Assumptions and overview of the T&L model

In duplicating the T&L model mathematically, we have found it necessary to understand unambiguously all of its assumptions. These assumptions are listed in Table 1 as a comprehensive summary, and are discussed in more detail in sections that follow. Considering the intricacies of nitrogenase catalysis, engendered by the fact that not one, but two component proteins comprise the enzyme system, as well as by the fact that there are various possible reductants and substrates to nitrogenase, a list of all of the assumptions built into a comprehensive nitrogenase model is multifaceted. We have therefore attempted to categorize the assumptions in Table 1 within a framework of the categories: protein activity; reductant source; Fe protein cycle; and MoFe protein cycle.

Schemes 1 and 2 show kinetic pathways of the Fe protein cycle, assuming slightly different mechanisms, and they should be considered companions to the appropriate category in Table 1. Similarly, Scheme 3 should be considered alongside the MoFe protein cycle category of Table 1. The rate constants for *Klebsiella pneumoniae* nitrogenase in Schemes 1–3 are summarized in Tables 2a and 2b, a compilation of information from various sources [5,17,19]. Rate constants specific to the original T&L schemes (Schemes 1 and 3, excluding acetylene pathways) are listed in Table 2a, to be distinguished from additional pathways that were determined at a later time (Scheme 2 and the acetylene pathways in Scheme

Table 1
Fundamental assumptions of the T&L model

Assumption category	Specifics
Protein activity	Only Kp nitrogenase is modeled by the T&L model; it may be shown that Schemes 1–3 describe nitrogenase from other organisms, although with different rate constants
	Only irreversible effects of protein inactivation are taken into account, not reversible effects from such sources as salt and CO
	Kp1 or E_n refers to MoFe protein active sites, taken from the Mo content of a Kp1 solution
	Inactive Kp1 does not interact with Kp2
	Inactive Kp2 competes with active Kp2 for Kp1, binding with the rate constants k_3 and k_{-3}; Kp2 is 45% active
Reductant source	Dithionite (DT) is modeled as the initial reductant source
	—A two-electron transfer is not considered, as Kp2 functions only in the $[Fe_4S_4]^{2+}/[Fe_4S_4]^{1+}$ redox couple with DT as reductant
	—The actual reductant of DT solutions is the SO_2^- radical, so the K_{obs} of reducing Kp2 is proportional to the square root of DT concentration
	The reduction of $Kp2_{ox}(MgADP)_2$ is the only significant DT–Kp2 interaction
	Nucleotide exchange following reduction is rapid compared to k_4
	[ATP] is far in excess compared to [ADP]
Fe protein cycle	All explicit assumptions of Scheme 1 for the classical T&L model, or Scheme 2 for the modern/integrated T&L model
	–Of particular note, the k_{-3} pathway is irreversible for the transition of E_{n+e} to E_{n+1}
	–The k_{-3} pathway is rate-limiting in catalysis, except under conditions of very low protein concentration, in which case the k_1 pathway is rate-limiting
	–The rate constants k_5 and k_{-5} do not enter into this scheme
	Only Kp2 not bound to Kp1 is capable of being reduced
	One completion of the Fe protein cycle accounts for the transfer of a single electron to Kp1
MoFe protein cycle	All explicit assumptions of Scheme 3, where straight dashed arrows represent a single Fe protein cycle
	–Of particular note, $E_4N_2H_2$ derived only from E_4H_4 is allowed to back-react with H_2 to form E_4H_4 in the k_{-11} pathway
	The rate constants of the Fe protein cycle are assumed to be independent of the level of reduction of Kp1
	Only free Kp1 is capable of binding substrate and releasing product
	Henry's law determines the concentration of aqueous gas substrates
	Quench releases a single H_2 from all E_2H_2 and E_3H_3 species and from free $E_2H_2C_2H_2$, and two H_2 from E_4H_4. N_2H_4 is released from $E_4N_2H_2$ species. Two NH_3 equivalents are released from E_5 and E_6, and E_7 releases one NH_3 upon quenching. All $E_3HC_2H_4$ species yield C_2H_4 product upon quenching
	Natural NH_3 release is from E_6 and E_7
	At high protein concentrations, acetylene-bound Kp1 intermediates have different rate constants for binding Fe protein

Table 2
(a) Rate constants for the classical T&L model [5] and Additional rate constants for the modern/integrated T&L model [17,19]

Rate constant	Value	Comment
k_1	5×10^7 M^{-1} s^{-1}	Determined from the dilution effect [15]
k_{-1}	15 s^{-1}	
k_2	200 s^{-1}	Determined by difference in ε for $Kp2_{red}$ and $Kp2_{ox}$ [20]
k_3	4.4×10^6 M^{-1} s^{-1}	Responsible for inhibition at high [Kp1] [12]
k_{-3}	6.4 s^{-1}	Rate-limiting step in catalysis [12]
k_4	3.0×10^6 M^{-1} s^{-1}	Reduction by SO_2^- and nucleotide exchange [12]
k_5	4.4×10^6 M^{-1} s^{-1}	Used when MgATP, but not reductant, is limiting [12]
k_{-5}	6.4 s^{-1}	— not in any of the simulations of the present work
k_6	1.2×10^9 M^{-1} s^{-1}	$SO_4^{2-} \underset{k_6}{\overset{k_{-6}}{\rightleftarrows}} 2SO_2^{2-}$ [12]
k_{-6}	1.75 s^{-1}	
k_7	250 s^{-1}	Subject to errors of a factor of approximately 2 [5]
k_8	8.0 s^{-1}	
k_9	400 s^{-1}	
k_{10}	4×10^5 M^{-1} s^{-1}	Determined from $K_{m_{N_2}}$ at low e^- flux [13–16]
k_{-10}	8×10^4 M^{-1} s^{-1}	Determined from $K_{i_{H_2}}$ at low e^- flux [13–16]
k_{11}	2.2×10^6 M^{-1} s^{-1}	Determined from $K_{m_{N_2}}$ at low e^- flux [13–16]
k_{-11}	3×10^6 M^{-1} s^{-1}	Determined from $K_{i_{H_2}}$ at high e^- flux [13–16]
(b)		
$k_{2,e}$	176 s^{-1}	Set to 200 s^{-1} to simulate classical model
$k_{2,ATP}$	50 s^{-1}	Set to 10^9 s^{-1} to simulate classical model
$k_{2,Pi}$	22 s^{-1}	Set to 10^9 s^{-1} to simulate classical model
$k_{2,cycle}$	1.5 s^{-1}	Set to 0 s^{-1} to simulate classical model
k_{12}	10^7 M^{-1} s^{-1}	Determined from
k_{-12}	100 s^{-1}	K_s for C_2H_2 [17]
k_{14}	400 s^{-1}	C_2H_4 release [17]

3), as listed in Table 2b. This categorization corresponds to two different states of the T&L model: (1) the model as it was first developed (designated here as the *classical T&L model*); as opposed to (2) the model in its present state (designated here as the *modern / integrated T&L model*).

2.1. Protein activity

Thorneley and Lowe are meticulous about correcting for active vs. inactive protein, so that their simulations match their experimental reaction stoichiometry. The nitrogenase enzyme system can be particularly susceptible to inactivity, because both the Fe and MoFe proteins undergo post-translational insertion of metal cofactors essential for maximal protein activity [5]. Incomplete insertion leads to the presence of inactive apo protein. In addition, other factors, such as natural enzyme degradation, oxygen inactivation and sensitivity to temperature, can also lead to irreversible protein inactivity, and certain substances reversibly inhibit protein activity, e.g. binding of CO to the FeMo cofactor, competing with the reduction of some substrates [17], as well as high salt concentrations, which prevent Fe–MoFe protein complex formation [21,22].

While there may be a number of effects contributing to enzyme inactivity, corresponding to a variety of types of protein inactivation, it is simplest to consider overall effects of inactive proteins that apply to all cases. These effects include irreversible inactivation, rather than reversible in-

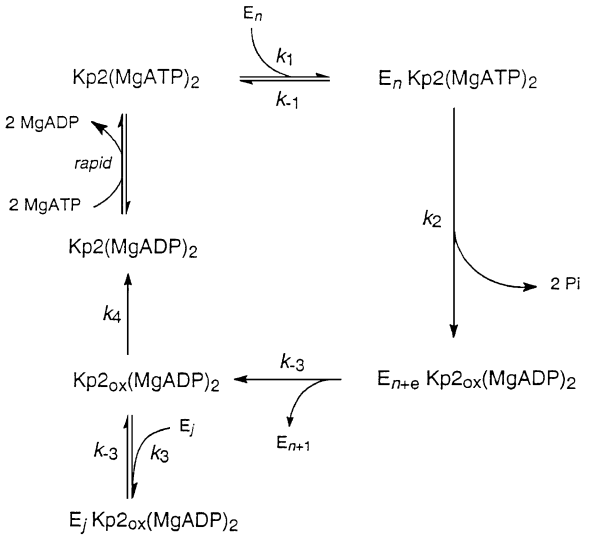

Scheme 1. Caption for scheme 1.

activation, which cannot be described currently within the strictly mathematical framework of the T&L model. Inactive apo Kp1 is assumed not to interact with Kp2 at all, because it lacks the FeMo cofactor [5]. Because each Kp1 contains two independently operating halves, each with a FeMo cofactor, the Mo content of Kp1 is taken as a measure of active sites, a value twice the molar protein concentration for fully active MoFe protein. When cited below, Kp1 represents Mo content (active site concentration), and not molar MoFe protein concentration.

Both active and inactive forms of Kp2 possess an $[Fe_4S_4]$ cluster that functions using the $[Fe_4S_4]^{2+}/[Fe_4S_4]^{1+}$ couple. Inactive Kp2 is assumed to compete with active Kp2 for Kp1, binding with the same affinity as $Kp2_{ox}(MgADP)_2$ [5,12]. The T&L model assigns active Kp2 a specific activity of 3500 nmol C_2H_4 min^{-1} mg^{-1} at 30°C, consistent with 45% active protein, an assignment that was necessary for Thorneley and Lowe to simulate pre-steady-state progress curves for H_2, N_2H_4 and NH_3 product formation [5]. The remaining 55% inactive Kp2 is assumed to compete with the active Kp2 for Kp1.

2.2. Direction of electron flux

The overall kinetics of nitrogenase catalysis proposed in the T&L model requires three interdependent sets of redox reactions involving interactions of different types of electron carriers and the directional flux of electrons from one type of carrier to another. These interactions are in the order of: (1) electron source → Fe protein; (2) Fe protein → MoFe protein; and (3) MoFe protein → substrates.

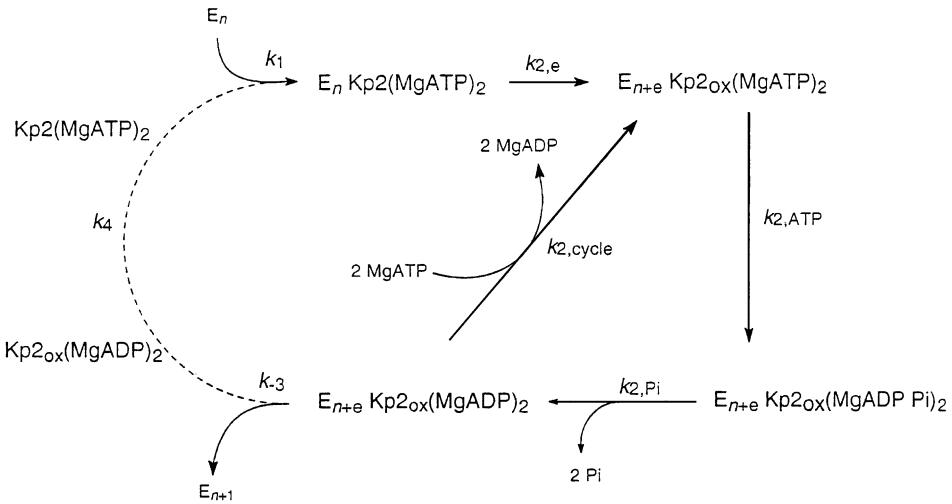

Scheme 2. Caption for scheme 2.

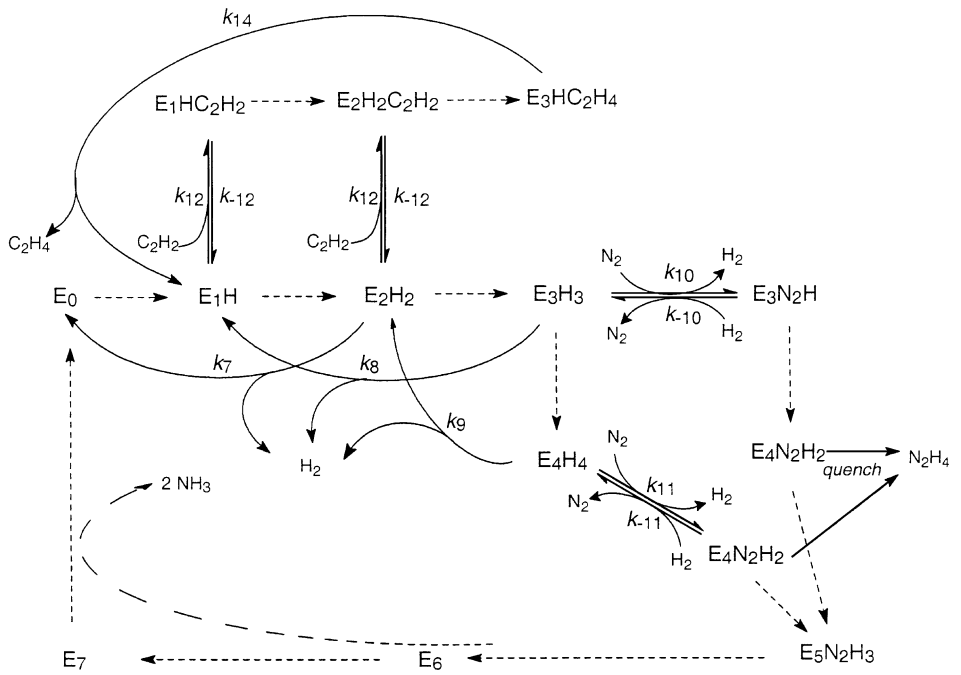

Scheme 3. Caption for scheme 3.

2.2.1. Reductant requirement: electron source → Fe protein

Nitrogenase requires a low-potential source of electrons, such as dithionite (DT), Ti^{3+}-citrate, or methyl viologen in vitro, and possibly flavodoxin or ferredoxin in vivo. The choice of electron source can have a significant impact on the overall kinetics of nitrogenase, because both the $[Fe_4S_4]^{2+}/[Fe_4S_4]^{1+}$ and $[Fe_4S_4]^{0}/[Fe_4S_4]^{2+}$ redox couples can function during catalysis [4,23–25], and which couple is active is dependent on the reductant type and its concentration. The T&L model was developed using DT as reductant, and consequently, the T&L model applies only to the use of the $[Fe_4S_4]^{2+}/[Fe_4S_4]^{1+}$ redox couple. Because commercial sodium dithionite is only partially pure (50–85%), it is necessary for precise kinetic studies to purify it [26] or to standardize it by titration against standardized oxidants, such as FMN or $K_3Fe(CN)_6$ [5]. Regardless of the purity of the reductant, its overall concentration must not exceed certain reductant-dependent limits, beyond which salt concentration inhibits Fe–MoFe protein interactions. For DT, this is approximately 20–30 mM [27]. The actual reductant of DT solutions is not $S_2O_4^{2-}$, but the SO_2^- radical formed by dissociation [28]:

$$S_2O_4^{2-} \overset{K_6}{\leftrightarrow} 2SO_2^-$$

$$2SO_2^- + H_2O \leftrightarrow HSO_3^- + H^+ + e^-$$

The rate of Fe protein reduction by SO_2^- is dependent on the presence of nucleotides and is slowest in the presence of MgADP [5], although this is the only Kp2 reduction reaction in the T&L model:

$$2SO_2^- + OH^- + Kp2_{ox}(MgADP)_2 \overset{k_4}{\rightarrow} HSO_3^- + Kp2_{red}(MgADP)_2$$

Once the Fe protein is reduced, it is assumed that nucleotide exchange occurs rapidly compared to the reduction of Kp2:

$$Kp2_{red}(MgADP)_2 + 2MgATP \xrightarrow{fast} Kp2_{red}(MgATP)_2 + 2MgADP$$

The affinity of reduced Fe protein for MgATP is smaller than that for MgADP [4], so for nucleotide exchange to be complete, it is implicit that the amount of MgATP is in large excess compared to MgADP. This condition is satisfied for in vitro reactions conducted in the presence of the ATP regenerating system, as well as for early time scales of in vitro assays lacking a regenerating system. In either case, the effect of varying ADP concentration cannot be gauged within the strict framework of the model, as this violates the condition of rapid nucleotide exchange.

2.2.2. Fe protein cycle: Fe protein → MoFe protein

Only reduced Kp2 bound to two MgATP is capable of transferring an electron to Kp1, so the association of $Kp2_{red}(MgATP)_2$ and Kp1 is the first in a series of pathways leading to substrate reduction, which is exclusive to the component proteins of nitrogenase. The relationship of this k_1 pathway with its complement k_{-1} is measured by varying k_{-1}/k_1 to get a best-fit simulation of Schemes 1 and 3 to dilution effect data found in figure 3 of reference [5], having already determined all the other rate constants in Table 2a. These same data and simulation are displayed in Fig. 1 of this publication, along with our duplication, which will be discussed later in more detail.

The k_2 pathway leads to electron transfer with concomitant hydrolysis of two ATPs. While it has been shown that ATP hydrolysis is not required for electron transfer, the rate of ATP-independent electron transfer is insignificant compared to the rate of electron transfer coupled to ATP hydrolysis [29]. Likewise, electron transfer is not required for ATP hydrolysis [5,30,31]. Therefore, determining if there is a rigid sequence of these events has been of interest for a number of years. Originally, the T&L model did not attempt to make this distinction, so the k_2 pathway could not account for reductant-independent ATP hydrolysis, nor could real-time phosphate release from the Kp2–Kp1 protein complex be modeled. More recently, Lowe et al. [19] modified the ki-

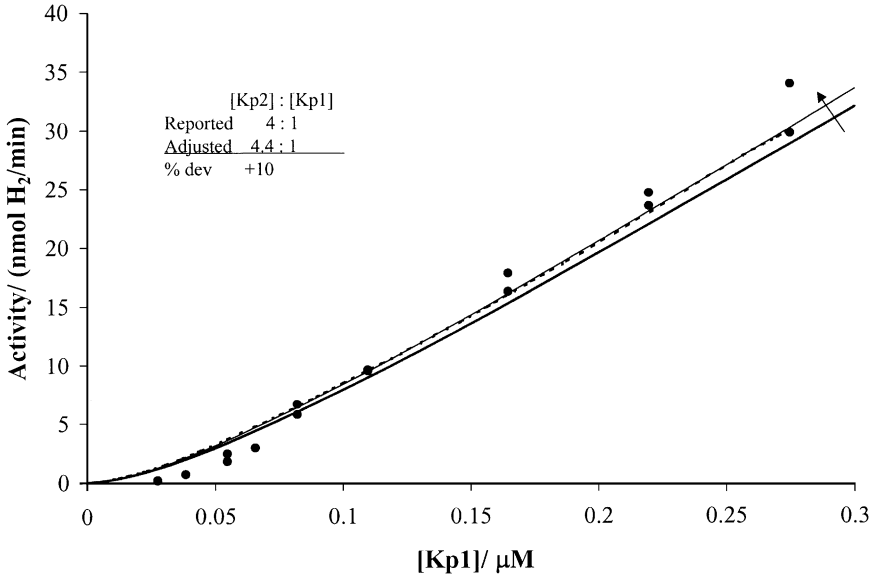

Fig. 1. Dilution effect at a constant Fe/MoFe ratio of 4: 1, T&L data (●) at pH 7.4 and 23°C, and original simulated best-fit curve (-----) of the classical T&L schemes to the data to solve for k_{-1}/k_1 [5,13]. [DT] is 10 mM, and [ATP] is 9 mM. Additional lines are for our duplication effort, with reported and adjusted protein ratios (thick line → thin line, respectively) as indicated in the table inset.

netic scheme of the Fe protein cycle to account for both of these effects, as in Scheme 2. For convenience in describing the different steps within the k_2 pathway, we have adopted the notation $k_{2,e}$ to represent electron transfer. This is followed by ATP hydrolysis, $k_{2,ATP}$, and then by phosphate release, $k_{2,Pi}$. The order of these events was determined by fitting a kinetic scheme to data of pre-steady-state phosphate release [19], whereas the original value of k_2 was measured spectroscopically from differences in the extinction coefficients of reduced and oxidized Fe protein during nitrogenase turnover [5]. Note that there is also a pathway in Scheme 2 for ATP to replace ADP in the Fe–MoFe protein complex, so that the T&L model can explain reductant-independent ATP hydrolysis. This pathway is designated here as $k_{2,cycle}$.

The type of nucleotide bound to the Fe protein affects the stability of the Kp1–Kp2 complex. After ATP hydrolysis and phosphate release, $Kp2_{ox}(MgADP)_2$ dissociates from Kp1. This k_{-3} pathway is rate-limiting in the Fe protein cycle (except for very small protein concentrations, which make the k_1 pathway rate-limiting) [12]. Once freed from Kp1, oxidized Kp2 has less affinity for Kp1 than reduced Kp2, yet under conditions of low electron flux through nitrogenase from an increase in the Kp1/Kp2 protein ratio, the expected activity of Kp2 is compromised by the re-association of oxidized Kp2 with Kp1 in the k_3 pathway. This phenomenon is referred to as 'MoFe inhibition', because excess MoFe protein inhibits the reduction of oxidized Fe protein. By varying the concentration of Kp1 in experiments to measure DT turnover from Kp2 reduction, the rates k_3 and k_{-3} were measured [12]. Since these experiments were performed in the absence of ATP, it was also determined that $Kp2_{red}(MgADP)_2$ binds Kp1 with the same affinity as $Kp2_{ox}(MgADP)_2$, so that $k_5 = k_3$ and $k_{-5} = k_{-3}$, as in Table 2a. We have previously noted, however, that one of the important assumptions of the T&L model is that ATP concentration must be in excess compared to ADP concentration, and that nucleotide exchange on reduced Kp2 is rapid. Therefore, the rate constants k_5 and k_{-5} do not actually enter into any of the kinetic schemes presented in this work.

Only free $Kp2_{ox}$ is capable of being reduced in the k_4 pathway. The reason for this can be deduced from the T&L explanation of MoFe inhibition — if $Kp2_{ox}$ is bound to Kp1, then its Fe–S cluster is unexposed to reductant-containing solvent. Furthermore, the Fe–S cluster must be the site of Kp2 reduction, as well as the site of electron transfer to Kp1. After Kp2 reduction, the Fe protein cycle starts over.

2.2.3. The MoFe protein cycle: MoFe protein → substrate

One completion of the Fe protein cycle accounts for the transfer of one electron from Kp2 to Kp1. However, all nitrogenase substrates require $2n$ electrons, $n \geq 1$. For example, the reduction of N_2 to $2NH_3$ (with obligatory reduction of at least $2H^+$ to H_2) involves the transfer of at least eight electrons (or eight Fe protein cycles). The MoFe protein cycle accounts for various reduction levels of Kp1/substrate complex before a particular substrate is released as product, as in Scheme 3 (combined schemes from Lowe and co-workers [16,17], with certain assumptions made more explicit [14]). In this scheme, E_n represents one of two independent halves of the MoFe protein, where n indicates the level of reduction, and E_0 corresponds to the level of reduction of Kp1 isolated in the presence of DT. By assuming that the constants of the Fe protein cycle are independent of the level of reduction of Kp1 [16,32], the T&L model has the potential to be applied easily to any possible substrate, although this has only been done so far with H^+, N_2, and C_2H_2, as indicated in Scheme 3.

In the absence of alternative substrates, nitrogenase reduces H^+ to H_2. After the first reduction of Kp1 by Kp2 — and after the dissociation of $Kp2_{ox}(MgADP)_2$ — the FeMo cofactor of Kp1 interacts with solvent, and a metal hydride is formed: E_1H [17]. Subsequent reduction cycles result in the binding of more hydrides. After the second reduction, Kp1 is in the E_2H_2 reduction state and is capable of evolving H_2. Therefore, the observations of the Hageman and Burris lag-

phase experiment are built into the T&L model [5,9]. Only free Kp1 is assumed to be capable of evolving product, so, for example, if reduced Kp2 binds E_2H_2 before H_2 is released, E_3H_3 can be generated. This assumption was deduced from the observation that the lag phase of product evolution from E_2 vs. E_3 or higher levels of reduction actually increases with increasing Kp2 concentration [16]. The maximum reduction level of Kp1 where H^+ is the only substrate is assumed to be E_4H_4.

Thorneley and Lowe determined much of their data through a combination of rapid acid-quench experiments and stopped-flow spectroscopy [16]. Whereas natural product evolution comes from free Kp1 only, acid quench releases substrate intermediates from both free Kp1 and the Kp2–Kp1 protein complex. By modeling pre-steady-state kinetic data with these techniques, Thorneley and Lowe gain insights into the nature of substrate intermediates. Specifically, all E_0 and E_1H species release no product upon quenching, although the latter has one electron equivalent present. The quenching of all E_2H_2 and E_3H_3 intermediates, on the other hand, releases a single H_2 molecule, and E_4H_4 releases two H_2. Therefore, the total H_2 evolution measured in the rapid acid-quench technique originates from both quenching and natural product evolution, as reported in figure 8 of reference [5]. (See also Fig. 2 of this publication, which includes our duplication of quenching versus natural H_2 release.) However, it is important to note exactly when one intermediate becomes another, so as to correctly assign which species release product upon quenching. Specifically, E_2H_2 is formed immediately after the first release of $Kp2_{ox}(MgADP)_2$ from the E_1H-class $E_{1+e}H$, and is considered E_2H_2, even after electron transfer, until the same Kp2 protein that reduced it is released. This idea is made explicit in Scheme 1, where E_{n+e} represents an E_n species that has been reduced, yet has not had its Kp2 released so as to allow its FeMo cofactor to interact with solvent. Once this

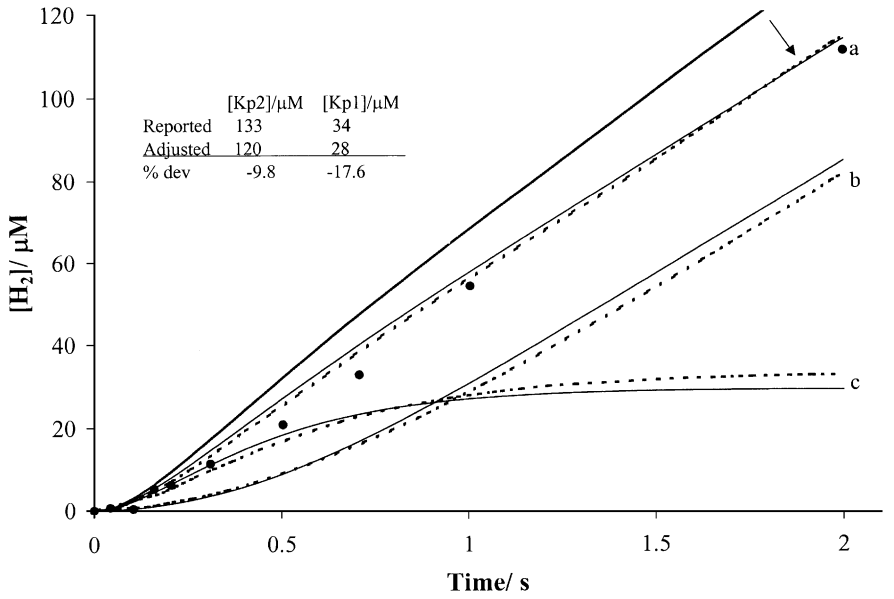

Fig. 2. Pre-steady-state reduction of H^+ in the absence of N_2 and C_2H_2. H_2 from different sources: (a) total product from natural release and release upon acid quench; (b) natural release from enzyme; and (c) release upon acid quench from species E_2, E_3 and E_4. T&L data (●) at pH 7.4 and 23°C, and original simulation (-----) of the classical T&L schemes [5]. [DT] is 10 mM, and [ATP] is 9 mM. Additional lines are for our duplication effort, with reported and adjusted protein concentrations (thick line → thin line, respectively) as indicated in the table inset.

dissociation occurs, E_{n+e} is considered an E_{n+1} species rather than an E_n species. From this, it is evident that the T&L model emphasizes the idea that only free MoFe protein can interact with and reduce substrate.

Henry's law is used to determine the concentration of gaseous substrates, such as N_2, in solution. The presence of N_2 leads to an overall decrease in H_2 evolution, as more of the electron flux goes towards generating NH_3 (compare fig. 11 with fig. 10 in reference [5]). However, H_2 evolution is never completely stopped experimentally, even at very high pressures of N_2 [33]. This observation is built into Scheme 3 as the obligatory release of H_2 from E_3 and E_4 upon binding of N_2. Furthermore, under lag-phase conditions (low overall component protein concentrations, and/or large Kp1/Kp2 ratios), E_3 and E_4 are not formed to any significant extent, and the experimental H_2/N_2 product ratio approaches infinity, supporting the correctness of the absence of N_2 binding to Kp1 of reduction levels below E_3 in Scheme 3.

Just as the first reduction state of Kp1 with a bound hydride (E_1H) is assumed to release no product upon quenching, the first reduction state of Kp1 bound to N_2 (E_3N_2H) releases no H_2 or NH_3 products upon quenching. However, $E_4N_2H_2$ releases hydrazine (N_2H_4) upon either acid or base quench, assuming that the extra two electrons required to obtain N_2H_4 from $E_4N_2H_2$ come from 'super-oxidation' of Kp1 [5,14]. Yet Thorneley and Lowe were only able to match pre-steady-state N_2H_4 release if $E_4N_2H_2$ derived only from E_4H_4 is allowed to back-react with H_2 to form E_4H_4 in the k_{-11} pathway, whereas $E_4N_2H_2$ derived from E_3N_2H is not allowed to form E_4H_4. The basis for this assumption is that both hydrides in E_4H_4-derived $E_4N_2H_2$ are bound to the cofactor, whereas E_3N_2H-derived $E_4N_2H_2$ has undergone irreversible protonation of the N_2 intermediate itself [14]. This assumption is made explicit in Scheme 3. Figure 12 of reference [5] shows a simulation of hydrazine formation with these assumptions in place. (Our duplication of this figure can be found in Fig. 4, to be discussed in greater detail later on.) The T&L model is not definitive on which intermediates naturally release NH_3, although one possibility is that NH_3 is released from E_6 and E_7, so that two NH_3 equivalents are bound to E_5 and E_6 for release upon quenching, and that E_7 releases one NH_3 upon quenching [14]. Scheme 3 is not explicit on this point because of other possibilities for NH_3 release. These assumptions are built into our duplication of figure 13 of reference [5], corresponding to Fig. 5 in this publication, to be discussed later.

As with N_2 reduction, C_2H_2 binds Kp1 at two possible reduction levels. For C_2H_2, these are E_1 and E_2. However, Scheme 3 is only valid if used to simulate conditions of low protein-component concentrations. For concentrations necessary to generate data from the rapid acid-quench technique, Lowe et al. observed that Kp nitrogenase activity was much lower than expected [17], so they proceeded to fit their data to a simplified scheme for acetylene reduction, valid only for higher protein concentrations. Several important conclusions were drawn from this analysis. First, quenching of free $E_2H_2C_2H_2$ yields H_2 and C_2H_2, whereas this same species with bound Kp2 releases no product upon quenching. All $E_3HC_2H_4$ species are presumed to yield C_2H_4 upon quenching. Perhaps more important than knowing which products are released upon quenching, is an explanation for why the observed activity of acetylene reduction is much lower than expected at the high protein concentrations required to simulate the data taken with the rapid acid-quench technique. An analysis of this inactivity using their simplified scheme, along with the observation that at low protein concentrations this inactivity is not observed, led Lowe and coworkers to postulate that the inactivity is due to an increase in the association rates of component nitrogenase proteins, k_3, and not in their dissociation [17].

3. Duplicating the classical T&L model

With a thorough understanding of the assumptions of the T&L model, from the time of its inception until the present, we have been able not only to duplicate published results, but also to

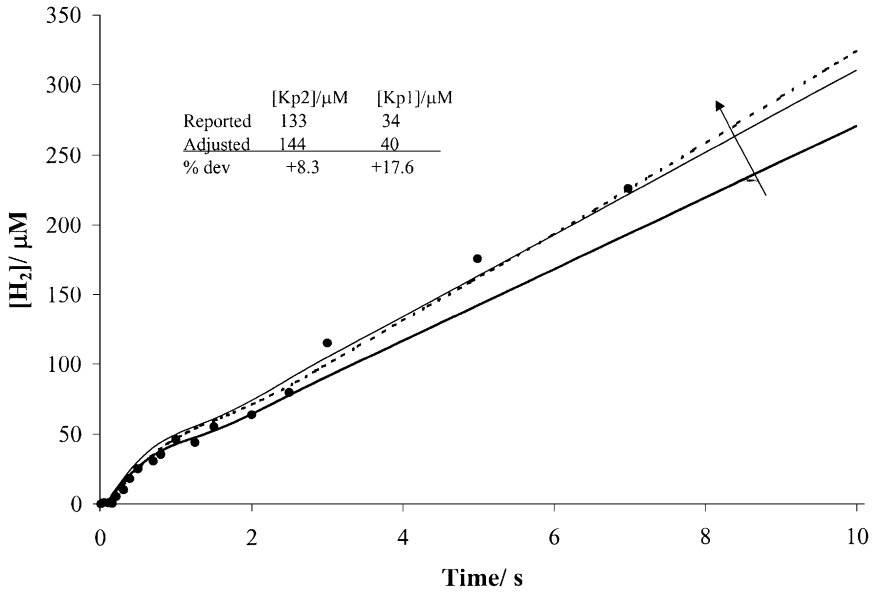

Fig. 3. Pre-steady-state H_2 evolution from natural and acid quench sources, with nitrogenase under 100% N_2. T&L data (●) at pH 7.4 and 23°C, and original simulation (-----) of the classical T&L schemes [5,16]. [DT] is 10 mM, and [ATP] is 9 mM. Additional lines are for our duplication effort, with reported and adjusted protein concentrations (thick line → thin line, respectively) as indicated in the table inset.

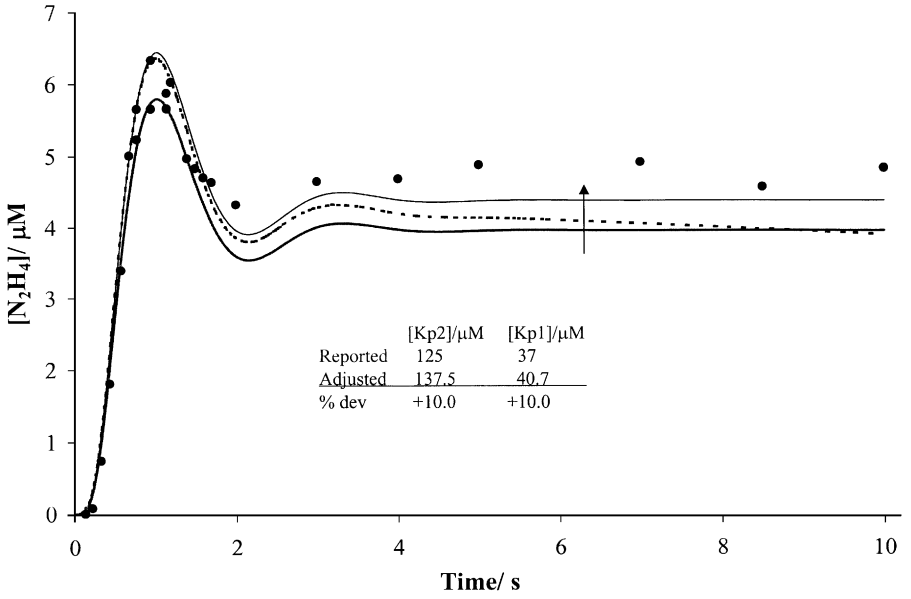

Fig. 4. Pre-steady-state N_2H_4 release upon acid or base quench of nitrogenase under 100% N_2. T&L data (●) at 23°C, and original simulation (-----) of the classical T&L schemes [5,14]. [DT] is 10 mM, and [ATP] is 9 mM. Additional lines are for our duplication effort, with reported and adjusted protein concentrations (thick line → thin line, respectively) as indicated in the table inset.

predict Kp behavior under experimental conditions beyond what has been previously published. This has been accomplished using the information in Tables 1, 2a and 2b and Schemes 1–3, in the strictly mathematical framework of a computer program written in the MATHEMATICA programming language. This program is capable of simulating a wide variety of experimental conditions, and the code itself in the form of a MATHEMATICA file is available as supplementary material, alongside commentary and examples to enable ready use by other groups.

Even with all of the assumptions up until the present, however, it is instructive to suspend consideration of more recent additions to the T&L model in an attempt to more closely duplicate the original (classical) T&L model published from 1983 to 1985 [5,12–16]. Selected original published data and simulations of the classical T&L model were digitized using UN-SCAN-IT gel software, from references as indicated in Figs. 1–5. These were then used as targets for our MATHEMATICA simulations. Original data are plotted as points and the original T&L simulations are given as dashed lines. The thick solid line is the MATHEMATICA simulation based on the same conditions (protein component concentrations or ratios) stated in the original publications. We are not always able to duplicate original T&L simulations precisely using their published protein concentrations. However, one of the assumptions of the T&L model is that protein concentrations can be adjusted for simulations to correct for experimental error in the data. The thin solid line in these figures represents an adjusted fit after varying protein concentrations. An arrow indicates the direction of activity change required to adjust initial simulations to better-fit simulations, and a table insert to each figure indicates the percent variation between corresponding 'reported' and 'adjusted' conditions.

Fig. 1 displays the dilution effect of Kp nitrogenase at a constant [Kp2]/[Kp1] ratio. The T&L simulation of the data (dashed line) is actually a best-fit curve used to solve for the value of k_{-1}/k_1, having already determined the other rate

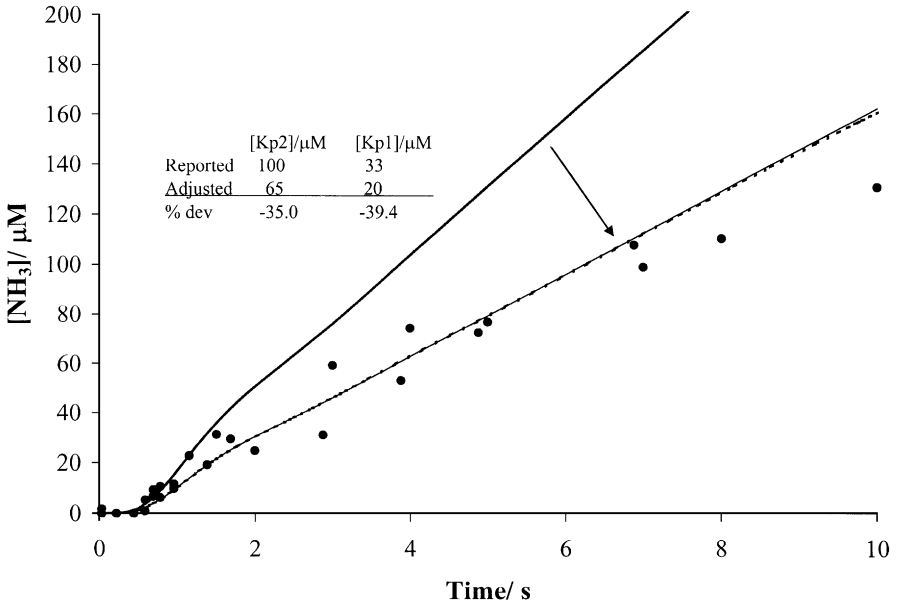

Fig. 5. Pre-steady-state NH_3 release from natural release and acid quench of nitrogenase under 100% N_2. T&L data (●) at pH 7.4 and 23°C, and original simulation (-----) of the classical T&L schemes [5,14]. [DT] is 10 mM, and [ATP] is 9 mM. Additional lines are for our duplication effort, with reported and adjusted protein concentrations (thick line → thin line, respectively) as indicated in the table inset.

constants in Table 2a [5,13]. Our initial simulation of the dilution effect at the reported [Kp2]/[Kp1] ratio of 4:1 shows a [Kp1]-dependent deviation from the T&L simulation. Because this particular simulation varies the protein concentrations while keeping the protein ratio constant, any error in component protein concentrations is propagated as an error in protein ratio. It would seem, therefore, that any error in the protein ratio would be dependent on protein concentration. By allowing this ratio to vary by 10%, we obtain an excellent match of the original simulation.

Whereas the simulations of Fig. 1 involve steady-state kinetics, where product from acid quenching is negligible compared to natural product release, much of the power of the T&L model resides in simulating pre-steady-state kinetics, where product from acid quench must be accounted for. This is illustrated in Fig. 2. Curve (a) describes total H_2 release under argon and apportions it between natural release (b) and H_2 released upon quenching of enzyme intermediates (c). Only total product formation is shown for our duplication of this data at the reported protein concentrations, for purposes of greater clarity in the figure, but each of the component sources of H_2 evolution in our simulation are more active for original concentrations than they are for adjusted concentrations. Note the time-dependent positive deviation from the original T&L simulation. Allowing the enzyme component concentrations to vary from those reported gives good agreement with the experimental and T&L simulation for total H_2 release. However, this is only achieved if curve (b) possesses a small, time-dependent deviation towards too much product compared to the original T&L simulation, whereas curve (c) deviates towards too little H_2 formation upon acid quenching. These deviations are small and probably not serious. Of greater concern is the fact that our adjusted MoFe protein concentration had to be decreased by 17.6% compared to the reported concentration, well beyond the limit of $\pm 10\%$ variance indicated in Table 1. This result is particularly interesting in light of our success in simulating the dilution effect in Fig. 1, considering that what is simulated in each case is H_2 release in the absence of N_2. In Fig. 1, simulated product formation at the reported concentration was not active enough, whereas in Fig. 2, even natural product formation at reported concentrations is too active.

Fig. 3 shows pre-steady-state release of H_2 from nitrogenase in the presence of 100% N_2. There is an initial burst of H_2 formation, followed by a near-linear production of H_2 with time. For this linear region of product formation, our initial simulation at the reported protein concentrations is not active enough, contrary to the discrepancy in the absence of N_2, as in Fig. 2, where it is too active. By allowing the protein concentration to vary, the MATHEMATICA simulation comes into agreement with the experimental data and the T&L simulation. Unfortunately, as with the adjusted simulation in Fig. 2, this is only possible if MoFe protein concentration deviates by 17.6%. Yet this deviation must not be considered a systematic difference between our computer program and that of Thorneley and Lowe, considering that adjusted MoFe protein concentration was *decreased* in Fig. 2, yet *increased* in Fig. 3. Therefore, this inconsistency must be due to some other reason.

It is conceivable that the reason our simulations in Figs. 2 and 3 fail to precisely match the published T&L simulations within the $\pm 10\%$ limits of the model is that their simulations were not performed strictly within this parameter. However, there is also a possibility that there are key differences or errors in the way the differential equations describing Schemes 1–3 have been encoded in the two separate programming formats. We conjecture that the T&L simulations do not carefully encode certain differential equations in terms of conservation of mass, leading to certain problems in their simulations. That this is a plausible argument is illustrated by fundamental differences between our simulations and that of Thorneley and Lowe in Fig. 4, which reports the pre-steady-state production of N_2H_4 formed by acid or base quench of nitrogenase under 100% N_2. Of particular note is that in our MATHEMATICA simulations, at both reported and adjusted concentrations, the quantity of N_2H_4 released on quenching levels off after approximately 4 s, whereas the original T&L simulation

displays a notable negative drift away from the data points. What is most interesting about this difference is that our simulation at adjusted protein concentrations within the ±10% limits of the model actually match the original T&L data better than does the original T&L simulation, as displayed by both an elevated activity in the steady-state region after 4 s, and an absence of negative drift away from the data at higher time scales, which is present in the original T&L simulation. An attempt to fit the original T&L simulation directly was also successful only up to the 4-s mark (not shown) within the ±10% limits of the model, at which point our simulation maintained gentle oscillations about a steady-state concentration, with a marked decrease in amplitude over time. Fig. 4 is most telling for the success of our computer program, as we go beyond an attempt merely to match an original T&L simulation and focus instead on how close it comes to matching actual experimental data within the parameters of the model.

The failure of the MATHEMATICA model to match activities within the ±10% limits in Figs. 2 and 3 is continued in Fig. 5, in contrast to the success of our adjusted simulation in Figs. 1 and 4. Fig. 5 is a pre-steady-state progress curve for NH_3 evolution from nitrogenase under 100% N_2, with total product originating from both natural and quenched sources (as has been the case for other pre-steady-state simulations as well). Because the data in Fig. 5 were obtained with similar protein concentrations to those in Figs. 2 and 3, similar simulation behavior of electron flux should be observed. Fig. 5 shows that the MATHEMATICA simulation predicts a much greater activity than that actually measured, or even simulated originally by Thorneley and Lowe. In order to obtain agreement with the original T&L data and simulation, the Kp2 and Kp1 concentrations had to be adjusted by 35 and 39.4%, respectively — well beyond the accepted variation of up to 10% for each protein. However, when this large adjustment is made, exceptionally good correspondence for the T&L and the MATHEMATICA simulations is obtained. In order to evaluate this large discrepancy, we performed an internal consistency check for our program by executing the simulations of Figs. 2, 3 and 5 at [Kp1] = 34 μM and [Kp2] = 133 μM and compared the total electron flux through nitrogenase in the absence (Fig. 2) and presence (Figs. 3 and 5) of N_2. This analysis revealed that in the presence of N_2, our simulated nitrogenase is approximately 7% more active than in its absence. While this may contradict the observed phenomenon for Av that electron flux through nitrogenase is actually decreased by 13% in the presence of N_2 [34], this 7% theoretical increase is intuitive in terms of the original T&L kinetic schemes. First, consider that in the presence of N_2, there are additional pathways that release product faster than in its absence. For instance, there is obligatory release of H_2 upon binding of N_2 in the k_{10} and k_{11} pathways. Also, there is no indication of extra rate constants for the release of product NH_3 from nitrogenase in addition to the rate constants of the Fe protein cycle, e.g. k_{-3}. On the other hand, H_2 release must correspond to the additional rate constants k_7, k_8 and k_9, whereas NH_3 release in Scheme 3 is assumed to be automatic (fast) with the completion of an Fe protein cycle upon $Kp2_{ox}(MgADP)_2$ release. This behavior is built into the T&L schemes to increase the electron flux through nitrogenase in the presence of N_2 gas and is consistent with a higher activity for NH_3 formation, such as in our initial simulation at reported concentrations in Fig. 5. It would seem, therefore, that the data and published T&L simulation reflect a lower enzyme activity than corresponds to the expected activity from Scheme 3.

The classical T&L model is also an able predictor of other nitrogenase catalytic reactions under conditions other than those we have just examined. For instance, The T&L model was used to predict the relative amounts of E_0 and E_1 under lag-phase conditions to show that the first two Fe protein cycles occur at identical rates for Kp [32]. It was also used to simulate the effect of Kp2/Kp1 ratio on the apparent K_m of N_2 fixation [15]. We have duplicated this particular simulation, as shown in the inset to Fig. 6. Additionally, we report theoretical values for the V_{max} of NH_3 production at protein ratios corresponding to those of our duplication of apparent K_m. These inset curves to Fig. 6 were obtained by per-

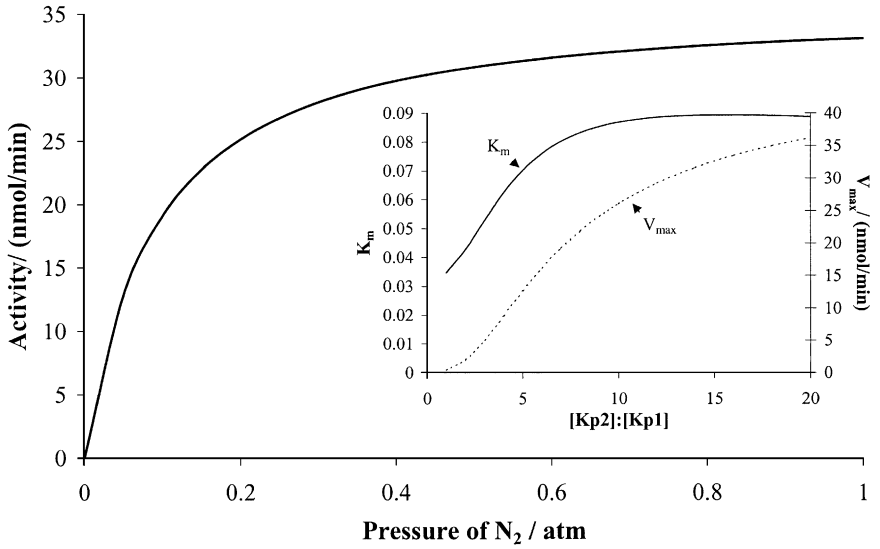

Fig. 6. Theoretical Michaelis–Menten kinetics for varying the pressure of N_2 at constant protein concentrations [Kp1] = 0.57 μM, [Kp2] = 11.4 μM (thick line). Insets indicate effects of varying protein ratio at constant [Kp1] = 0.57 μM on the observed K_m (thin line) [5,15] and V_{max} (dotted line). Note the last points in the inset plots are derived from the Michaelis–Menten plot.

forming simulations of varying N_2 pressure at various protein concentrations, and performing a curve fit to solve for K_m and V_{max} for each of the chosen protein concentrations, as in the main curve in Fig. 6. Other uses of the classical T&L model include various pre-steady-state and steady-state kinetic simulations published previously [5,12–16,18], including effects of varying the input parameters [DT], pressure of N_2, pressure of H_2, and concentrations of any form of Fe and MoFe proteins and/or intermediates. We shall not attempt to perform every possible simulation to prove that we have duplicated the T&L model. Rather, we have paid particular attention to pre-steady-state kinetic simulations and activities of major products evolved during nitrogenase catalysis (Figs. 2–5), assuming that the host of variant simulations that the program can perform stem from or are similar to those we have presented.

4. Classical T&L model vs. modern/integrated T&L model

In spite of its success, the classical T&L model has its limitations, some of which were partially overcome by later additions to the model, including pathways for acetylene reduction [17] and phosphate release [19]. We will refer to our duplication of the T&L model that includes these additional pathways as the *integrated* or *modern* T&L model. As there are few published experimental examples for Kp nitrogenase involving the new pathways of the modern T&L model, much of what follows are theoretical predictions based on Schemes 2 and 3.

4.1. Phosphate release

When the Fe protein cycle is expanded to include pathways for ATP hydrolysis and phosphate release, as in Scheme 2, the T&L model is able to predict the sequence of events of electron transfer and ATP hydrolysis, and fit pre-steady-state phosphate release [19]. When Scheme 2 is used in conjunction with Scheme 3, however, the extra pathways of Scheme 2 actually slow down simulated nitrogenase catalysis and introduce a longer lag phase before product release occurs, when compared to activities and lag phases when

Scheme 1 is used instead of Scheme 2. This is evidenced by a comparison of Figs. 2 and 7. In fact, in order for the Schemes 2 and 3 version of our program to match the Schemes 1 and 3 version, the extra rate constants of the k_2 pathway of Scheme 2 must be adjusted to the values indicated in Table 2b. Recall that in Fig. 2, adjusted Kp1 concentration varied from the reported concentration by 17.6%. On the other hand, adjusted Kp2 and Kp1 concentrations in Fig. 7 differ from the reported concentrations by only 10.5 and 11.8%, respectively. An even smaller deviation is possible if we attempt merely to match the slope (activity) of the original T&L simulation, and not the total product formation at the 2-s mark. Unfortunately, it is impossible for us to match the lag phase in the data and published T&L simulation very well, because even though k_{-3} remains rate-limiting in Scheme 2, the extra pathways slow down the Fe protein cycle too much for a better fit. This deviation from the data is perhaps acceptable, considering that it is comparable to the deviation of the simulation in Fig. 1 from the data in the dilution range below 0.08 μM. It is unlikely that any model of nitrogenase kinetics will match all observations exactly, so the small deviations of the integrated T&L model in product evolution are acceptable in consideration of its ability to predict more about nitrogenase kinetics, namely phosphate release.

4.2. Experimental vs. theoretical ATP / 2e values

In their attempt to simulate pre-steady-state phosphate release during nitrogenase catalysis [19], Lowe et al. did not attempt to describe elevated ATP/2e values, which Scheme 2 is capable of describing. Here we do so, but because we lack experimental data from Kp nitrogenase, we will limit our discussion to a qualitative comparison of what is known generally about nitrogenase from several organisms and what the integrated T&L model predicts about Kp nitrogenase.

The basic stoichiometry of nitrogenase catalysis requires the hydrolysis of a minimum of two ATPs for every electron transferred during the Fe

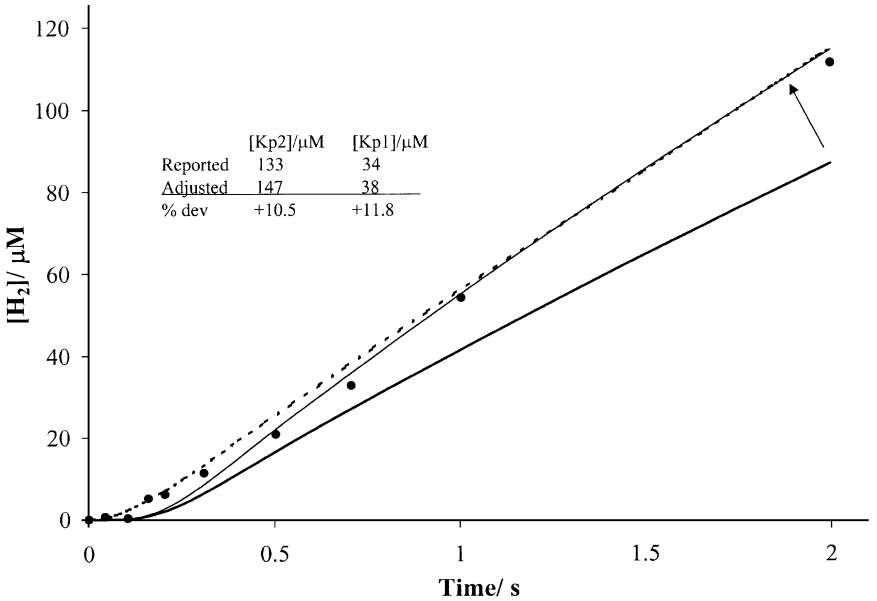

Fig. 7. Effects of including the integrated T&L model's k_2 pathways on total H_2 release. The same T&L data (●) and original simulation (-----) of the classical T&L schemes for total H_2 evolution, as in Fig. 2, is also given here [5]. [DT] is 10 mM, and [ATP] is 9 mM. Additional lines are for the duplication effort, including additional k_2 pathways, with reported and adjusted protein concentrations (thick line → thin line, respectively) as indicated.

protein cycle. Since electron transfer is measured by product release that requires $2n$, $n \geq 1$, electrons, a minimum of four hydrolyzed ATPs for every two electrons transferred is expected. As Scheme 2 indicates, ATP can be hydrolyzed without any electron transfer. Hence, the ATP/2e ratio becomes an important measure of the efficiency of nitrogenase catalysis for a variety of conditions. Experimentally, elevated ATP/2e values are observed under conditions of [5]: (a) lowered assay temperatures [35]; (b) using heterologous component proteins [31]; (c) limited reductant concentration [36]; limited electron flux through MoFe protein by (d) increasing Kp1/Kp2 [37,38]; and (e) the dilution effect [11]. Conditions (a) and (b) cannot be modeled using the integrated T&L model, but it is possible to explain qualitatively why they induce elevated ATP/2e in terms of Scheme 2. Since only the MoFe–Fe protein complex is capable of hydrolyzing ATP, anything that favors formation of the complex should increase the amount of ATP hydrolyzed relative to the number of electrons transferred. A lowered temperature as in (a) should have the effect of increasing the binding constant for the component proteins, as less kinetic energy is available to the MoFe–Fe protein complex for it to dissociate in the k_{-3} pathway. As the formation and maintenance of protein complex is favored by lowering temperature, we expect ATP/2e to increase. Likewise, heterologous protein components, e.g. Av1 and Cp2, lock together very tightly. They may hydrolyze ATP at a reduced rate [31], but the complex is strong enough to favor ATP hydrolysis over electron transfer.

Conditions (c), (d) and (e) can be modeled using our integrated computer program. Fig. 8 shows the effect of limiting the amount of reductant. In the absence of reductant, the Kp1–Kp2 protein complex is an ATPase [36], so we would expect ATP/2e to approach infinity as [DT] approaches zero. This is indeed the case in Fig. 8. What is interesting about Fig. 8 is at what concentration of DT we observe theoretical ATP/2e values approach the stoichiometric value of four. This occurs at the relatively low DT concentrations of less than 0.1 mM, whereas there is only very gradual change above 0.1 mM DT.

A more gradual increase in ATP/2e is observed for (d), where electron flux is limited by excess MoFe protein, as in Fig. 9. We intuitively expect the minimum ATP/2e value of 4 at a [Kp1]/[Kp2] ratio approaching zero, corresponding to excess Kp2 driving electron flux rapidly through Kp1.

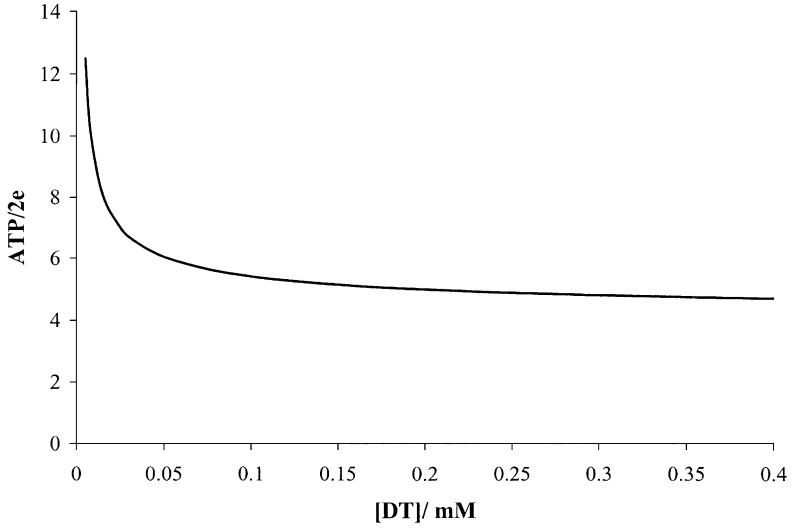

Fig. 8. Theoretical effects of DT dilution on the value of ATP/2e (or the ratio of the amount of Pi to the amount of natural H_2 evolved), simulated using the integrated T&L model with [Kp1] = 30 μM, [Kp2] = 30 μM, and [ATP] = 9 mM.

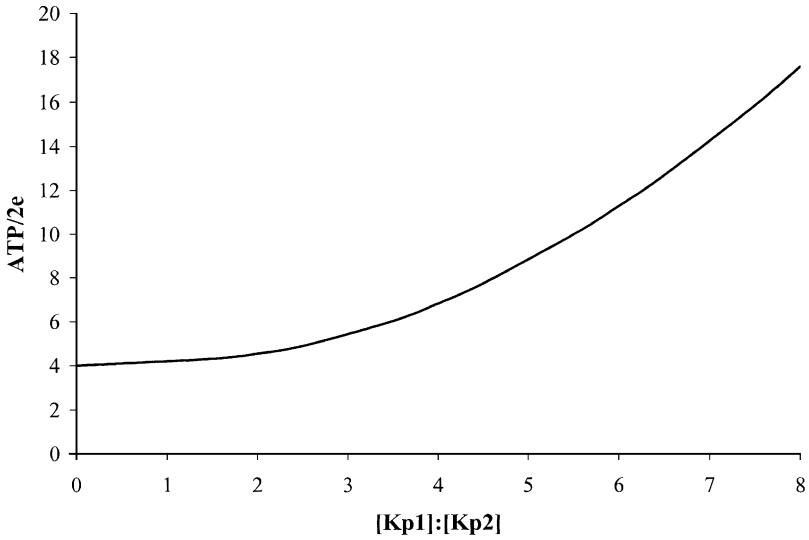

Fig. 9. Theoretical effects of [Kp1]/[Kp2] on the value of ATP/2e, simulated using the integrated T&L model with constant [Kp2] = 10 μM, [DT] = 10 mM, and [ATP] = 9 mM.

This is indeed the case, as shown in Fig. 9. At the other extreme, as [Kp1]/[Kp2] approaches infinity, we see that theoretical ATP/2e values continue to increase, as Kp2 is prevented from being reduced (k_4 pathway) because of competition with the k_3 pathway.

Finally, elevated ATP/2e values are also observed in the dilution effect for Av [11]. The dilution effect for Kp is displayed in Fig. 1, and predicted ATP/2e values can be found in Fig. 10. This behavior is qualitatively consistent with results from Av dilution experiments [11]. Our integrated T&L model does not predict significantly elevated ATP/2e values, except for very low protein concentrations. Note that the general trend at the far right in Fig. 10 is a slight, almost negligible increase in ATP/2e values with increasing protein concentrations. This is explained conceptually in terms of a greater likelihood of forming increasing concentration of ATPase-active Kp1–Kp2 complex by mass action, as well as by a decrease in the [DT]/[nitrogenase] ratio leaning towards limiting reductant at very high protein concentrations. The more significant increase in ATP/2e values at very low protein concentrations (less than 0.1 μM Kp1) must be due to a different phenomenon. We can rule out one possibility, which stems from the fact that at low protein concentrations, it takes longer for the nitrogenase enzyme system to reach steady state. Depending on which time frame is used as a reference for ATP/2e values, varied results are obtained. Note, for example, the simulated progress curve of ATP/2e vs. time in the inset to Fig. 10. Before product is ever released, ATP is already hydrolyzed, so predictably, the curve of ATP/2e vs. time is asymptotic with the ATP/2e axis. It is important to take the reference time in the far horizontal region of such a graph for each data point comprising the main graph in Fig. 10. Furthermore, as protein concentrations are lowered in the dilution effect, the time it takes for the real-time simulations to reach steady state increases, which is a reflection of electrons being tied up longer in Kp1 (because of less frequent interaction of Kp1 with Kp2) without being released as product, at least until a second electron is transferred to Kp1. Since the time it takes to reach steady state at low protein concentrations is longer, it is prudent to choose as a reference timeframe some time that well overestimates steady state to avoid time-dependent errors in the very low concentration range. For the main graph in Fig. 10, a reference time of 10 min is chosen,

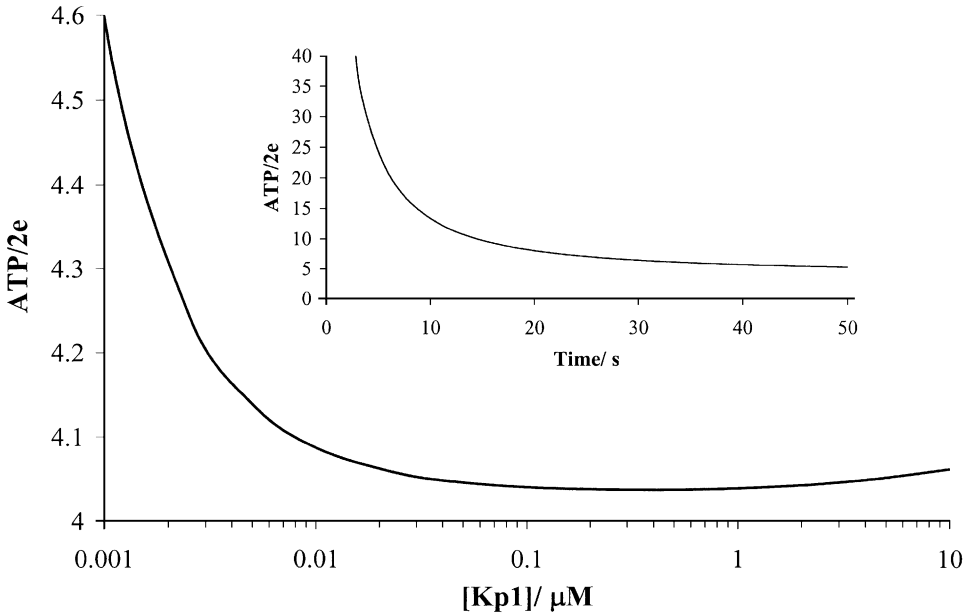

Fig. 10. Theoretical effects of protein dilution on the value of ATP/2e, simulated using the integrated T&L model with constant [Kp2]/[Kp1] = 4, [DT] = 10 mM, and [ATP] = 9 mM. Simulated assay duration was 10 min. Inset shows ATP/2e as a function of time at [Kp1] = 0.0005 μM.

and gives simulated data almost identical to the same conditions, but with a reference time of 50 s instead of 10 min. In other words, ATP/2e values converge on a steady-state value at large reference times. Because the graph indicates elevated ATP/2e values at very low concentrations — values that are also convergent, and hence reference time-independent — there must be some other factor that is primarily responsible for this elevation in ATP/2e values. While the obvious answer is that it is simply built into the mathematics of Schemes 1–3, specific causes for this increase are difficult to pinpoint.

4.3. Acetylene as substrate

Scheme 3 is sufficient to describe acetylene reduction at low protein concentrations, yet for the high concentrations required to simulate data taken using the rapid acid quench technique, Scheme 3 predicts a much more active rate of catalysis than is actually observed. The T&L model solves this problem by proposing a simplified scheme, which assumes a baseline Kp2 concentration and allows for different binding constants of $Kp2_{ox}(MgADP)_2$ to E_nH_n intermediates in the H_2-releasing pathway, as opposed to $E_nC_nH_n$ intermediates in the C_2H_4-releasing pathway [17]. An analysis of this simplified scheme led Lowe et al. to postulate that the decreased activity at high protein concentrations is due to an increase in the association rates of component nitrogenase proteins in the C_2H_4-releasing pathway, k_3, not in their dissociation [17]. With our integrated model, we are able to test this hypothesis. By increasing the value of k_3 for Kp1 bound to acetylene or an acetylene intermediate, we are able to bring the simulated activity of acetylene reduction down to experimental levels. Unfortunately, this occurs at the expense of H_2 evolution, which is much less active than it is experimentally. This problem could not be alleviated by varying component protein concentrations, suggesting that more than one rate constant (k_3 as well as others) must be different for acetylene reduction at high protein concentrations.

The value of this analysis has been a more direct test of initial conclusions and explanations.

4.4. Modeling multiple substrates

With the modern/integrated T&L model, we are able to evaluate many more effects than are possible with the classical T&L model. Whereas the T&L model has grown piece by piece, and has not been addressed as a single, unified whole, we are now able to do so. The foundation of any model rests in pre-steady-state kinetics. As an example, note the substrate-dependent distribution of electron flux for the three products simulated in Fig. 11 (H_2, C_2H_4, and NH_3). Each has a particular activity, as well as a particular lag phase, depending on the different interactions of reduced states of Kp1 for the various substrates. Yet steady state kinetics studies provide some tantalizing results as well. Fig. 12 shows theoretical effects of increasing the concentration of Kp1 at constant Kp2 concentration on the distribution of various products, including H_2, C_2H_4, and NH_3, as well as ATP/2e values. Note that NH_3 production is completely negligible under the simulated conditions. This is reasonable, since only under conditions of excess Kp2/Kp1 ratios are the concentrations of E_3 and E_4 sufficient for significant binding of N_2 to Kp1 in the k_{10} and k_{11} pathways. Since NH_3 production is of little significance under these conditions, the real interest of the figure shifts to the ideal Kp1/Kp2 protein ratio for reduction of H^+ vs. C_2H_2 by Kp1. While Fig. 12 appears to represent protein concentration-dependent competition of substrates for Kp1, the real issue is competition for various redox states of Kp1, where the distribution of Kp1 redox states is dependent on the Kp1/Kp2 protein ratio. On the other hand, Fig. 13 displays substrate competition for Kp1 at a single Kp1 and Kp2 concentration, so there is no variance in the distribution of the redox states of the MoFe protein. Rather, we can observe a direct inhibition of H^+ and N_2 reduction by increasing the simulated pressure of C_2H_2 above the reaction solution. Combining Figs. 12 and 13 into a 3-D plot would further elucidate the subtle effects of varying reaction conditions, particularly with regards to total protein concentration, not simply protein ratio. The possibilities of the integrated T&L model are many, so we have not attempted to portray a comprehensive illustration

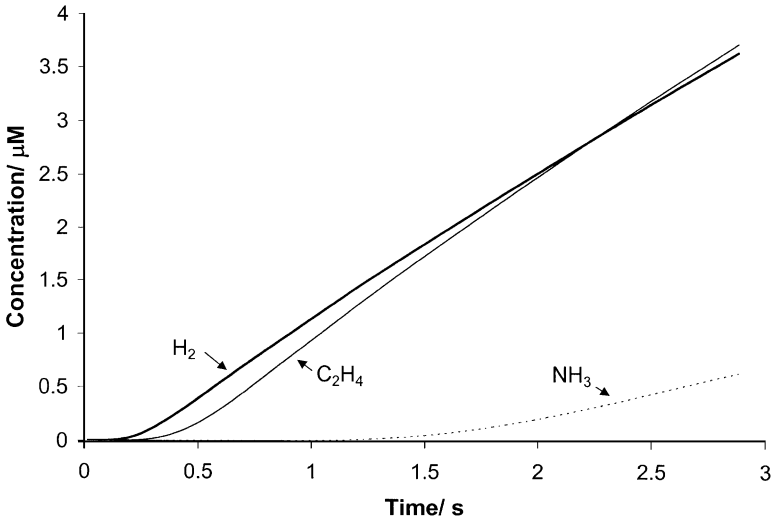

Fig. 11. Theoretical pre-steady-state natural product release: H_2 (thick line); C_2H_4 (thin line); and NH_3 (dotted line). The simulation uses the integrated T&L model with [Kp1] = 2 μM, [Kp2] = 8 μM, [DT] = 10 mM, [ATP] = 9 mM, 70% N_2, and 0.1% C_2H_2.

of its potential, but rather to portray just some of the possibilities. Whether our theoretical predictions actually match experimental data is yet to be seen, and could go a long way in validating the comprehensive nitrogenase kinetic model developed by Thorneley and Lowe.

5. Limitations of the T&L model: potential pitfalls in computer modeling

We have noted how versatile and comprehensive the T&L model is, particularly with the additional descriptions of ATP hydrolysis/phosphate release and acetylene reduction in its integrated/modern form. In performing simulations, however, the limitations of the model must be considered, as there are experimental observations that the model cannot explain.

We have already discussed the role of Kp nitrogenase component proteins in catalysis, as well as the effects of inactive proteins. In addition, we should note that other inhibitors of nitrogenase activity, including high salt concentration, ADP and CO, have not been modeled kinetically within the quantitative parameters of the T&L model. Deits and Howard successfully modeled kinetic effects of salt concentration on Av [22] with a scheme other than that used by T&L. Also, the effects of CO and ADP inhibition have been measured [17,36], but not modeled by fundamental kinetic pathways in the T&L model. Thus, inactivity brought about by the presence of these and other inhibitory agents is not modeled in this work. However, the serious user of the T&L model must also keep in mind that certain fundamental parameters of the model, if extended to extreme cases, lead to inhibitory conditions experimentally. For instance, modeling DT concentration beyond ~ 30 mM increases the rate of the k_4 pathway unrealistically, because at these concentrations, the salt concentration of DT itself would be experimentally inhibitory. Also, attempting to model extremely high component protein concentrations would unsuccessfully describe nitrogenase kinetics, as the experimental rate of ATP consumption would overpower the rate of ATP regeneration by an in vitro assay or in vivo system.

Sometimes substrate can even inhibit nitroge-

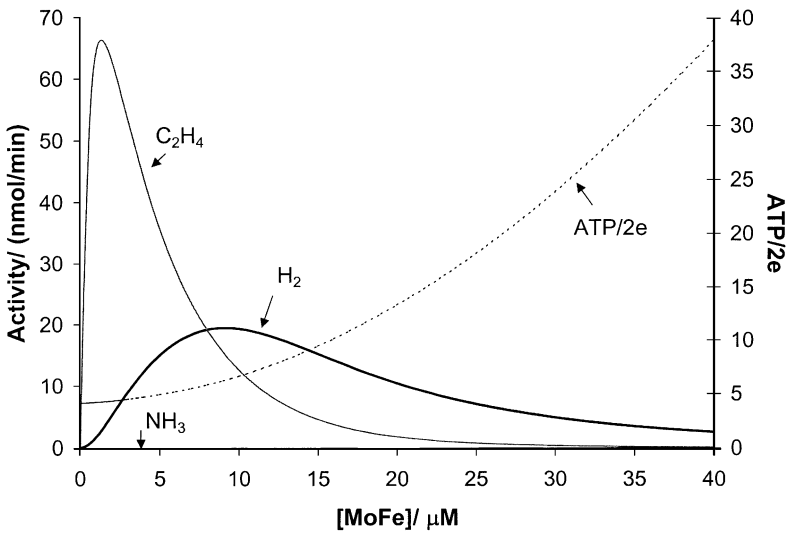

Fig. 12. Theoretical steady-state product distribution as a function of protein ratio: H_2 (thick line); C_2H_4 (thin line); and ATP/2e (dotted line). Note that NH_3 release is very close to zero for all indicated protein ratios. The simulation uses conditions of constant [Kp2] = 2 μM, [DT] = 10 mM, [ATP] = 9 mM, 70% N_2, and 30% C_2H_2.

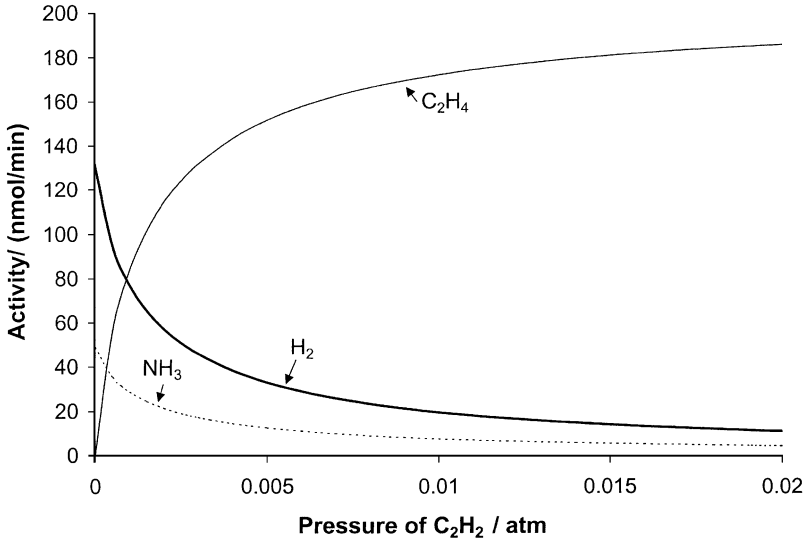

Fig. 13. Theoretical inhibition of H^+ and N_2 reduction as a function of increasing pressure of C_2H_2/H_2 (thick line); C_2H_4 (thin line); and NH_3 (dotted line). The simulation uses conditions of [Kp1] = 2 μM; [Kp2] = 8 μM; [DT] = 10 mM; [ATP] = 9 mM; and 70% N_2.

nase activity. We have already noted how at high protein concentrations, acetylene and acetylene intermediates bound to the MoFe protein change more than one of the rate constants in the Fe protein cycle, lowering overall activity. Therefore, the treatment of acetylene reduction with our computer program is valid only at low protein concentrations. For instance, the acetylene pathways of Scheme 3 worked for Lowe et al. at constant [Kp2] of 2 μM and [Kp1] of up to 20 μM, but were ineffectual at [Kp1] of 31 μM and [Kp2] of 124 μM [17].

Other limitations of the model are derived from the list of assumptions in Table 1. Most notably, the Fe protein cycle assumes rapid and complete nucleotide exchange in the k_4 pathway, which is only possible if [ATP] is far in excess of [ADP]. So, while Thorneley et al. propose a kinetic pathway for ADP inhibition of reductant-independent ATP hydrolysis [36], the determination of the proposed rate constant for this pathway cannot be determined within the parameters of the current T&L model, which lacks any consideration of [ADP] in the k_4 pathway. Furthermore, any attempt to simulate the observed effects of inhibition of nitrogenase catalysis by ADP by modifying the value of the k_4 rate constant is unsatisfactory and not quantitative.

A final consideration of simulating nitrogenase catalysis has to be in the numerical methods used to solve the number of simultaneous differential equations describing the various kinetic schemes. Any numerical technique is most accurate at small time scales, because even the slightest degree of error at the beginning of a simulation is magnified as time elapses, so that we must question the reliability of answers at large elapsed time. Such errors are evident in anomalous simulations, so they are generally easy to spot.

Acknowledgements

This research was supported by Grant 82-CRCR-1-1122 from the USDA/SEA Competitive Grants Program to G.D.W. and partially by the College of Mathematics and Physical Sciences at Brigham Young University. We also thank Dr David J. Lowe for helpful insights and comments about his nitrogenase kinetic model.

References

[1] W.G. Zumft, L.E. Mortenson, The nitrogen-fixing complex of bacteria, Biochim. Biophys. Acta 416 (1975) 1.

[2] B.E. Smith, R.R. Eady, Metalloclusters of the nitrogenases, Eur. J. Biochem. 205 (1992) 1.

[3] J. Kim, D.C. Rees, Nitrogenase and biological nitrogen fixation, Biochemistry 33 (1994) 389.

[4] B.K. Burgess, D.J. Lowe, Mechanism of molybdenum nitrogenase, Chem. Rev. 96 (1996) 2983.

[5] R.N.F. Thorneley, D.J. Lowe, Kinetics and mechanism of the nitrogenase enzyme systemin: T. Spiro (Ed.), Molybdenum Enzymes, 1, Wiley-Interscience, New York, 1985. p. 221

[6] B.K. Burgess, Substrate reactions of nitrogenasein: T. Spiro (Ed.), Molybdenum Enzymes, 1, Wiley-Interscience, New York, 1985. p. 161

[7] G.D. Watt, Z.C. Wang, R.R. Knotts, Redox reactions of and nucleotide binding to the iron protein of *Azotobacter vinelandii*, Biochemistry 25 (1986) 8156.

[8] F.J. Bergersen, G.L. Turner, Kinetic studies of nitrogenase from soybean root nodule bacteroids, Biochem. J. 131 (1973) 61.

[9] R.V. Hageman, R.H. Burris, Nitrogenase and nitrogenase reductase associate and dissociate with each catalytic cycle, Proc. Natl. Acad. Sci. USA 75 (1978) 2699.

[10] W.H. Orme-Johnson, L.C. Davis, M.T. Henzl et al., Components and pathways in biological nitrogen fixationin: W.E. Newton, J.R. Postgate, C. Rodriguez-Barrueco (Eds.), Recent Developments in Nitrogen Fixation, 1, Academic Press, London,, 1977. p. 131

[11] J.L. Johnson, A.C. Nyborg, P.E. Wilson, A.M. Tolley, F.R. Nordmeyer, G.D. Watt, Mechanistic interpretation of the dilution effect for *Azotobacter vinelandii* and *Clostridium pasteurianum* nitrogenase catalysis, Biochim. Biophys. Acta 1543 (2000) 36.

[12] R.N.F. Thorneley, D.J. Lowe, Nitrogenase of *Klebsiella pneumoniae*: kinetics of the dissociation of oxidized iron protein from molybdenum iron protein. Identification of the rate-limiting step for substrate reduction, Biochem. J. 215 (1983) 393.

[13] R.N. Thorneley, D.J. Lowe, The mechanism of *Klebsiella pneumoniae* nitrogenase action. Simulation of the dependences of H_2 evolution rate on component-protein concentration and ratio and sodium dithionite concentration, Biochem. J. 224 (1984) 903.

[14] R.N. Thorneley, D.J. Lowe, The mechanism of *Klebsiella pneumoniae* nitrogenase action. Pre-steady-state kinetics of an enzyme-bound intermediate in N_2 reduction and of NH_3 formation, Biochem. J. 224 (1984) 887.

[15] D.J. Lowe, R.N. Thorneley, The mechanism of *Klebsiella pneumoniae* nitrogenase action. The determination of rate constants required for the simulation of the kinetics of N_2 reduction and H_2 evolution, Biochem. J. 224 (1984) 895.

[16] D.J. Lowe, R.N. Thorneley, The mechanism of *Klebsiella pneumoniae* nitrogenase action. Pre-steady-state kinetics of H_2 formation, Biochem. J. 224 (1984) 877.

[17] D.J. Lowe, K. Fisher, R.N.F. Thorneley, *Klebsiella pneumoniae* nitrogenase mechanism of acetylene reduction and its inhibition by carbon monoxide, Biochem. J. 272 (1990) 621.

[18] D.J. Lowe, K. Fisher, R.N.F. Thorneley, *Klebsiella pneumoniae* nitrogenase pre-steady-state absorbance changes show that redox changes occur in the MoFe protein that depend on substrate and component protein ratio: a role for P-centres in reducing dinitrogen? Biochem. J. 292 (1993) 93.

[19] D.J. Lowe, G.A. Ashby, M. Brune, H. Knights, M.R. Webb, R.N.F. Thorneley, ATP hydrolysis and energy transduction by nitrogenasein: I.A. Tikhonovich, N.A. Provorov, V.I. Romanov, W.E. Newton (Eds.), Nitrogen Fixation: Fundamentals and Applications, 27, Kluwer Academic, London, 1995. p. 103

[20] R.N. Thorneley, Nitrogenase of *Klebsiella pneumoniae*. A stopped-flow study of magnesium–adenosine triphosphate-induced electron transfer between the component proteins, Biochem. J. 145 (1975) 391.

[21] A. Burns, G.D. Watt, Z.C. Wang, Salt inhibition of nitrogenase catalysis and salt effects on the separate protein components, Biochemistry 24 (1985) 3932.

[22] T.L. Deits, J.B. Howard, Effect of salts on *Azotobacter vinelandii* nitrogenase activities: inhibition of iron chelation and substrate reduction, J. Biol. Chem. 265 (1990) 3859.

[23] G.D. Watt, K.R.N. Reddy, Formation of an all-ferrous Fe_4S_4 cluster in the iron protein component of *Azotobacter vinelandii* nitrogenase, J. Inorg. Biochem. 53 (1994) 281.

[24] J.A. Erickson, A.C. Nyborg, J.L. Johnson et al., Enhanced efficiency of ATP hydrolysis during nitrogenase catalysis utilizing reductants that form the all-ferrous redox state of the Fe protein, Biochemistry 38 (1999) 14279.

[25] A.C. Nyborg, J.A. Erickson, J.L. Johnson, A. Gunn, S.M. Truscott, G.D. Watt, Reactions of *Azotobacter vinelandii* nitrogenase using Ti(III) as reductant, J. Inorg. Biochem. 78 (2000) 371.

[26] C. McKenna, W.G. Gutheil, W. Song, A method for preparing analytically pure sodium dithionite. Dithionite quality and observed nitrogenase-specific activities, Biochem. Biophys. Acta 1075 (1991) 109.

[27] J.L. Johnson, A.M. Tolley, J.A. Erickson, G.D. Watt, Steady-state kinetic studies of dithionite utilization, component protein interaction, and the formation of an oxidized iron protein intermediate during *Azotobacter vinelandii* nitrogenase catalysis, Biochemistry 35 (1996) 11336.

[28] R.N.F. Thorneley, M.G. Yates, D.J. Lowe, Nitrogenase of *Azotobacter chroococcum*: kinetics of the reduction of oxidized iron protein by sodium dithionite, Biochem. J. 155 (1976) 137.

[29] W.N. Lanzilotta, K. Fisher, L.C. Seefeldt, Evidence for electron transfer from the nitrogenase iron protein to the molybdenum–iron protein without MgATP hydrolysis: characterization of a tight protein–protein complex, Biochemistry 35 (1996) 7188.

[30] S. Imam, R.R. Eady, Nitrogenase of *Klebsiella pneumoniae*: reductant-independent ATP hydrolysis and the effects of pH on the efficiency of coupling of ATP hydrolysis to substrate reduction, FEBS Lett. 110 (1980) 35.

[31] C. Larsen, S. Christensen, G.D. Watt, Reductant-independent ATP hydrolysis catalyzed by homologous nitrogenase proteins from *Azotobacter vinelandii* and heterologous crosses with *Clostridium pasteurianum*, Arch. Biochem. Biophys. 323 (1995) 215.

[32] K. Fisher, D.J. Lowe, R.N.F. Thorneley, Klebsiella pneumoniae nitrogenase: the pre-steady-state kinetics of MoFe-protein reduction and hydrogen evolution under conditions of limiting electron flux show that the rates of association with the Fe-protein and electron transfer are independent of the oxidation level of the MoFe-protein, Biochem. J. 279 (1991) 81.

[33] J. Liang, R.H. Burris, Hydrogen burst associated with nitrogenase-catalyzed reactions, Proc. Natl. Acad. Sci. USA 85 (1988) 9446.

[34] S. Wherland, B.K. Burgess, E.I. Stiefel, W.E. Newton, Nitrogenase reactivity effects of component ratio on electron flow and distribution during nitrogen fixation, Biochemistry 20 (1981) 5132.

[35] G.D. Watt, W.A. Bulen, A. Burns, K.L. Hadfield, Stoichiometry, ATP/2e values, and energy requirements for reactions catalyzed by nitrogenase from *Azotobacter vinelandii*, Biochemistry 14 (1975) 4266.

[36] R.N.F. Thorneley, G.A. Ashby, C. Julius, J.L. Hunter, M.R. Webb, Nitrogenase of *Klebsiella pneumoniae*: reversibility of the reductant-independent magnesium ATP-cleavage reaction is shown by magnesium ADP-catalyzed phosphate–water oxygen exchange, Biochem. J. 277 (1991) 735.

[37] R.R. Eady, J.R. Postgate, Nitrogenase, Nature 249 (1974) 805.

[38] R.V. Hageman, R.H. Burris, Nitrogenase electron transfer and allocation and the role of ATPin: M.P. Coughlan (Ed.), Molybdenum and Molybdenum-Containing Enzymes, 1, Pergamon Press, New York, 1980. p. 403